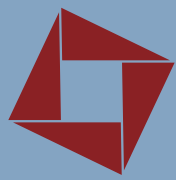


ICTS



INTERNATIONAL
CENTRE *for*
THEORETICAL
SCIENCES

NEWS

VOLUME IX
ISSUE 2
2023

TATA INSTITUTE OF FUNDAMENTAL RESEARCH

ASTROSAT: EIGHT YEARS ON AND COUNTING!



KULINDER PAL SINGH



September 28, 2015, 10 AM (IST) marks a historic moment when India joined the select group of nations with astronomical observatories in outer space.

The observatory called *AstroSat* is India's first satellite with a suite of co-aligned instruments to study stars and galaxies simultaneously in the Ultra-violet (UV)

and a broad range of energies in X-rays. It is, therefore, capable of addressing a large variety of topics in astronomy. Broadly speaking, its major scientific goals are *a) exploring the matter and emission processes in, and that swirling around, the deep gravitational fields of most dense objects like neutron stars, white dwarfs and black-holes, b) discovering star formation regions in galaxies, and c) finding the hot stars in young and old star clusters in our own galaxy.*

AstroSat payload weighing 1513 kg was injected into a near-equatorial and nearly circular orbit around the Earth with an

GRAVITATIONAL LENSING OF GRAVITATIONAL WAVES: A NEW FRONTIER OF ASTRONOMY

PARAMESWARAN AJITH

The 1919 observation of the gravitational bending of light heralded the remarkable success of general relativity (GR) in predicting and explaining a variety of astrophysical phenomena. During the 1919 solar eclipse, Arthur Eddington and colleagues confirmed that the bending of starlight by the gravitational field of the Sun is twice that predicted by the Newtonian theory of gravity, consistent with the GR prediction. This prediction has been further verified with remarkable accuracy by radio observations of distant quasars starting in the 1960s.

In the 1970s, astronomers started to observe more dramatic manifestations of the gravitational bending of light. Massive objects such as galaxies could focus light like an optical lens. The first of such observations was the multiple images produced by a gravitationally

... continued on Page 6 ...

apogee of ~650 kilometers and inclination of ~6° with respect to the equator. It was launched by Polar Satellite Launch Vehicle (PSLV-C30) from Sriharikota Range (SHAR)

north of Chennai on the eastern coast of India. It was then the heaviest and biggest satellite launched by a PSLV.

AstroSat has been observing, over the past eight years and over a range of wavelengths, and is therefore called a multi-wavelength observatory. Three Large Area X-ray Proportional Counters (LAXPC), a Soft X-ray focusing Telescope (SXT), and Cadmium–zinc–telluride Imager (CZTI) together cover a wide swath of X-ray energies from 0.3-200 keV. These three instruments were developed and deployed by a small group of academics and engineers in the department of Astronomy and Astrophysics at TIFR in collaboration with scientists in ISRO.

I led the development of SXT, India's first X-ray focusing telescope from 2001 onwards in collaboration with the University of Leicester, UK. The ultraviolet observations are carried out by two Ultra-violet Imaging Telescopes (UVIT) developed jointly by IIA, ISRO and IUCAA.

The two UV telescopes are aligned with the three X-ray instruments. One of them covers the near ultraviolet (NUV: 200-300nm) and visible wavelengths, and the other covers the far ultra-violet (FUV) band spanning 128-180nm. Visible channel is used only for tracking a source. Another X-ray instrument called the Scanning Sky

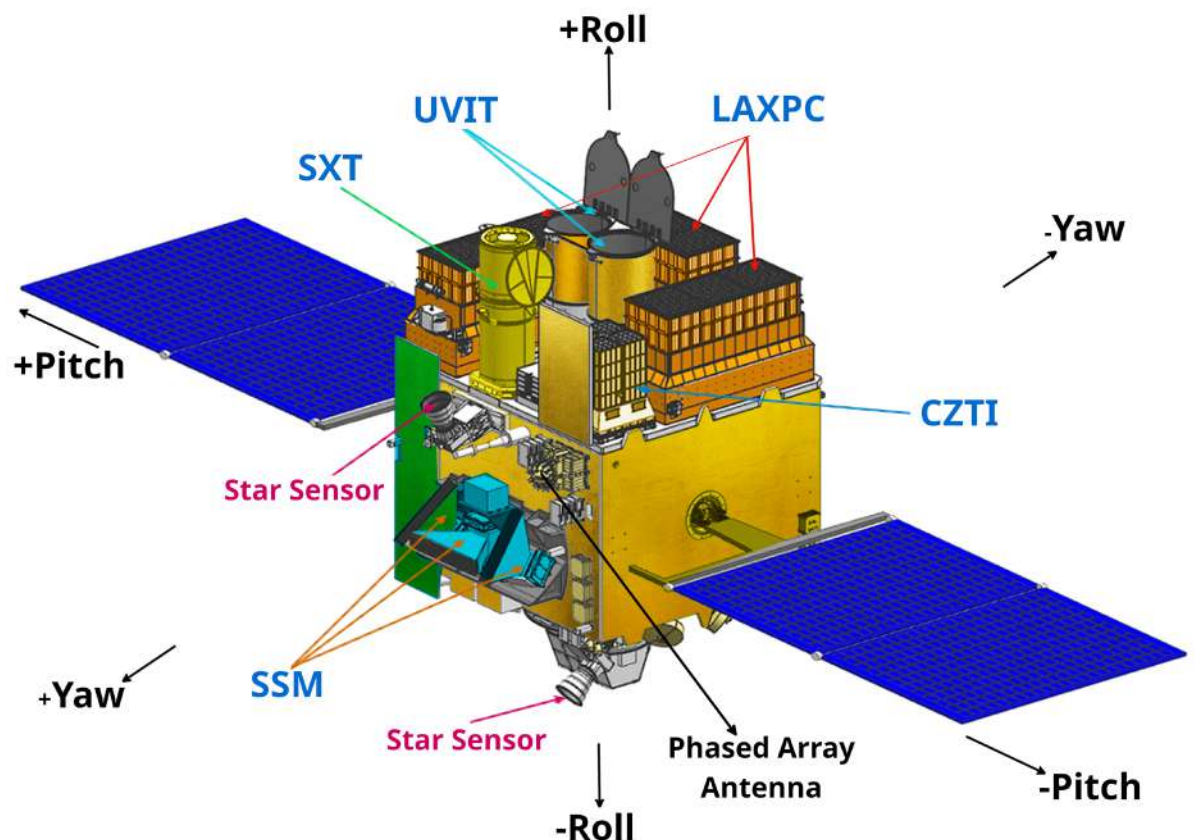


Figure 1: A schematic drawing of *AstroSat* showing all the detectors and telescopes. Credits: V. Girish, ISRO HQ, Bengaluru

Monitor (SSM) with three X-ray detectors mounted on a rotating platform oriented 90° with respect to the SXT, LAXPC, CZTI and UVIT scans the sky for transient sources that brighten suddenly. An auxiliary detector called Charged Particle Monitor (CPM) monitors the high energy charged particle background that can compromise

the observations by other instruments.

A schematic drawing of *AstroSat* and an actual photograph of the satellite after integration and before being coupled to the rocket are shown below in Figures 1 and 2 respectively. For more details on all the instruments, please refer to my article in the *Resonance* listed in the Bibliography.

AstroSat was opened to public at large in India and abroad after the first one-and-a-half years of verification phase by the instrument teams. The proposed observations are reviewed by the *AstroSat* Time Allocation Committee appointed by ISRO, and proposals selected based on scientific merit and technical feasibility are allotted. Many of the X-ray observations have a cadence of days to weeks.

AstroSat has carried out hundreds of observations over the last eight years, some of which have been augmented with simultaneous observations with other international astronomy satellites and ground-based observatories in the optical, radio, X-ray and gamma-rays. *AstroSat* has covered a wide range of subjects in astronomy. Many new findings with the *AstroSat* have been published with an overall rate of about one per week. Here, I shall give just a glimpse of some of the most important discoveries made with *AstroSat*. Some of these based on the first six years



Figure 2: Fully assembled *AstroSat* with folded solar arrays in a clean room in Shriharikota. Credits: ISRO

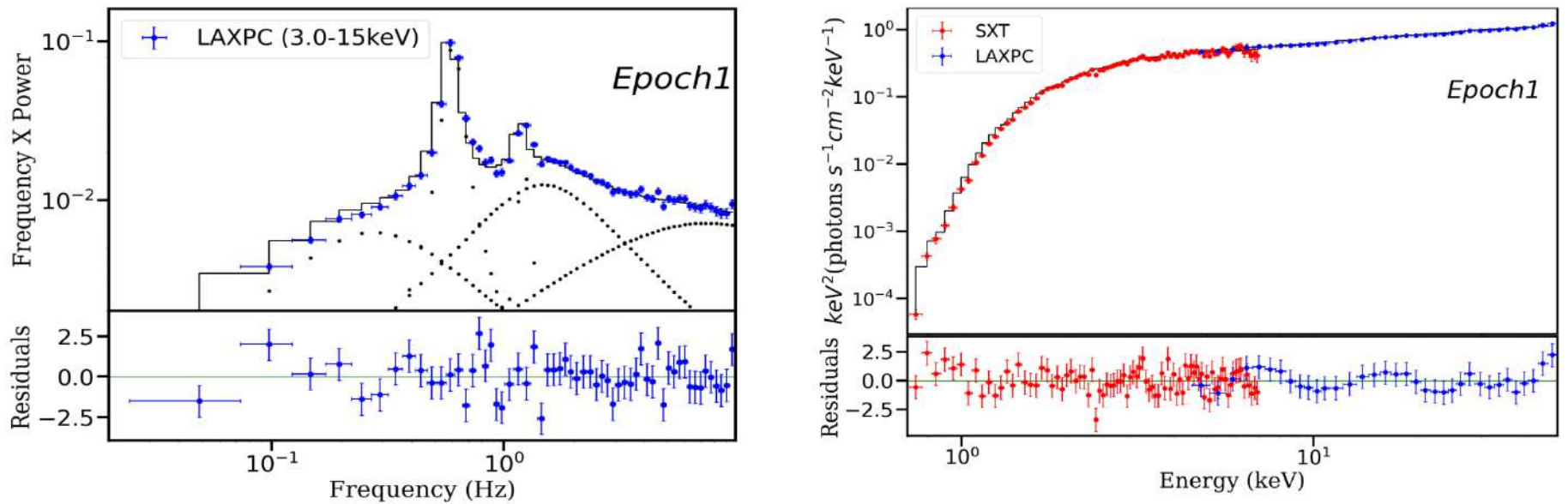


Figure 3: (left) The power density spectra obtained from the LAXPC, and (right) broadband spectra using LAXPC (blue) and SXT (red) in energy range of 0.7-50 keV for H 1743-322. Residuals from the best fit models are also shown. Credits: Husain et al 2023

of operations are also described in my publication in the *Resonance*.

One of the first significant observations was that of hard X-ray polarization of the Crab pulsar inside the Crab Nebula – a supernova remnant observed in 1054 AD. Measured at different rotation phases of the pulsar, this study published in *Nature* (Vadawale et al. 2018) suggests that the polarization shows maximum variation during the ‘off-pulse’ duration when no contribution from the pulsar is expected, challenging the current theories of X-ray production in the pulsar.

The high time resolution of the LAXPC has led to discovering the quasi-periodic behaviour in several accreting compact binaries systems harbouring stellar size black-holes in X-rays. At the same time the power of broad band X-ray studies combining the data from SXT and LAXPC reveals the intricacies of the emission processes in them.

One most recent example of this powerful aspect of *AstroSat* is shown in Figure 3 for a transient X-ray source H 1743-322, which is also a micro-quasar (Husain et al. 2023). LAXPC has also caught explosive burning on the surface of an accreting neutron star binary as Type-I bursts characterized by a sharp increase in X-ray intensity within 0.5-5.0 sec and an exponential decay in $\sim 10-100$ sec including burst oscillations at 581 Hz during the bursts (Roy et al. 2021).

SXT continues to extend the LAXPC spectra into the soft X-rays, and also independently continues to target soft X-ray sources like active stars and novae. Novae can continue

to glow for several days and months, after the initial outburst due to explosive nuclear burning from thermonuclear runaway process on the surface of a white dwarf (WD) which ejects and pushes the material from the surface at high velocities (>300 km/s). The expanding photosphere and the optically-thick ejecta around the WD result in a rapid increase in luminosity, and a complex ejecta. The steady nuclear burning continues on the WD surface

until the accrued fuel source is finished and the ejecta become optically thin and the photosphere recedes back to the WD starting to reveal strong emission peaking in soft X-rays known as the ‘super-soft X-ray source’. An example of emergence of such a stage was caught with the SXT for a recurrent nova, known as V3890 Sgr that erupted on 2019 August 27.87 after 28 years, is shown in Figure 4. These sources are believed to be the progenitors of Type

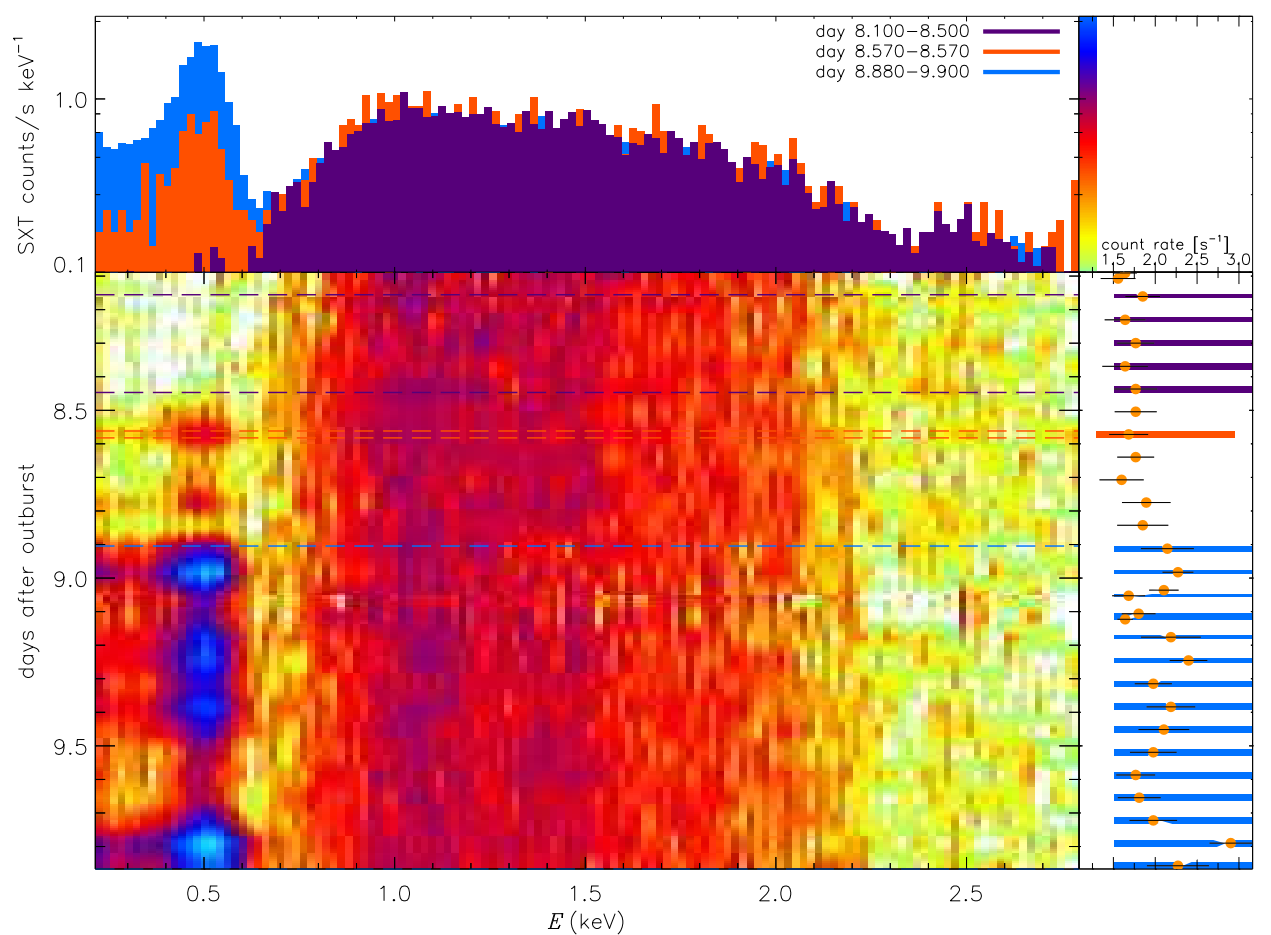


Figure 4: Soft X-ray spectral evolution of V3890 SgrA Recurrent Nova (recurrence time = 28 years) on hourly time scale on days 8-9 after the most recent outburst on 2019 August 27.87. Credits: Singh et al. 2021

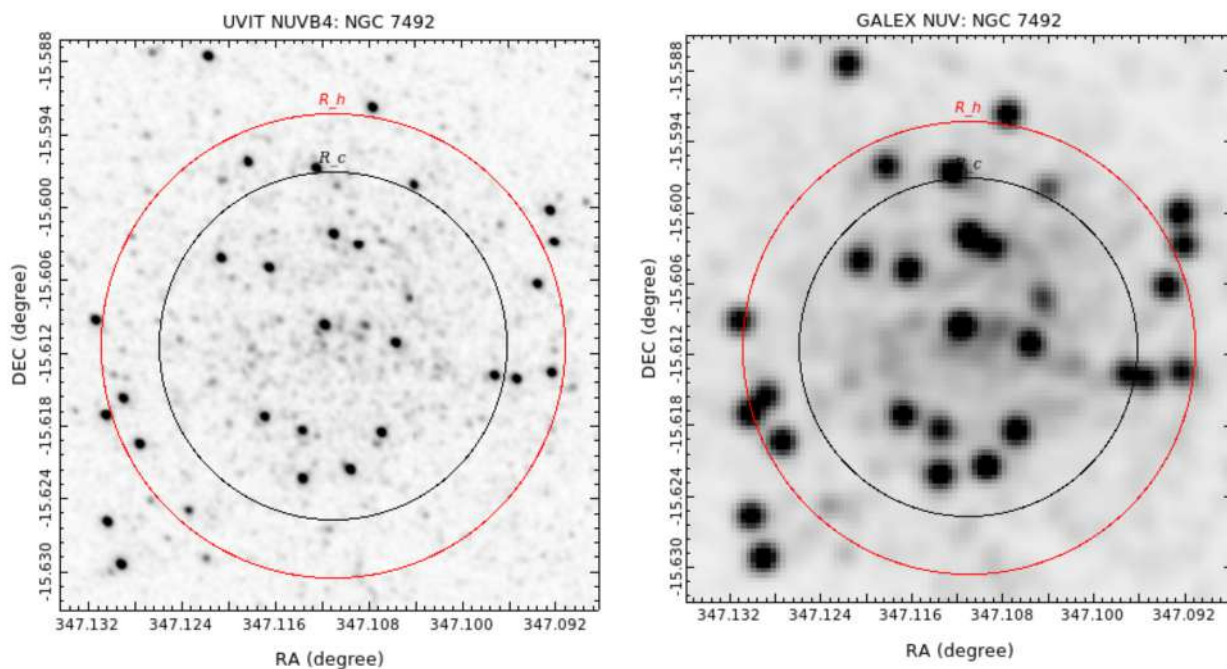


Figure 5: UVIT NUVB4 (263.2nm, left) and GALEX NUV (230.4 nm, right) images of a globular star cluster NGC 7492. The red circle denotes the half-light radius of 1.15 arcmin and the black circle denotes the core radius of 0.86 arcmin) of the cluster. Credits: Kumar, R. et al. (2021)

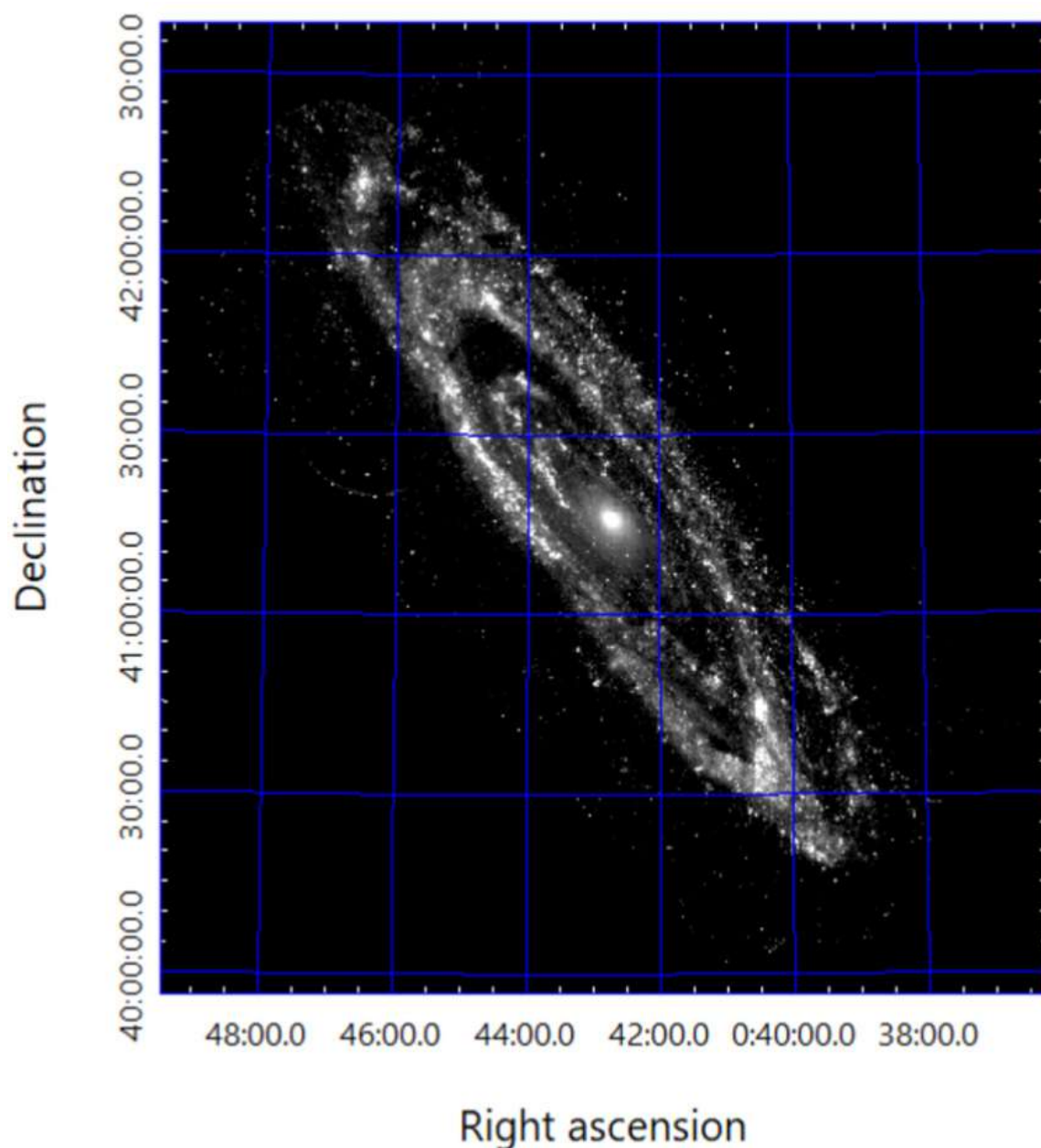


Figure 6: The FUV (148nm) mosaic of Andromeda made from 19 overlapping fields observed with the UVIT (Leahy et al 2023)

I supernovae used as standard candles for measuring distances and age of the universe.

The UVIT telescopes have a spatial resolution of 1.3 arcsec which is especially useful for studying fields crowded with hot UV emitting stars and to detect faint diffuse emission, thus placing it well ahead of its predecessor GALEX (Galaxy Evolution Explorer) which had spatial resolution of ~ 5 arcsec. A comparison of the quality of data obtained from UVIT NUV and GALEX NUV is shown in Figure 5 below (Kumar et al. 2021). The UVIT observations of NGC 7492 (Figure 5) also led to the discovery of a new extreme horizontal branch (EHB) star at the core of the cluster.

The mapping of Andromeda galaxy with UVIT (Figure 6) has not only produced a big catalog of hot stars in it but also to the discovery of 20 UV-emitting supernova remnants in Andromeda by virtue of UVIT's ability to resolve their diffuse emission (Leahy et al. 2023).

UVIT has carried out the deepest FUV survey of the Coma cluster of galaxies and has revealed a number of unusual looking galaxies with hitherto unseen FUV emission. An example is NGC 4907 shown in Figure 7. The difference in morphology of the young, UV emitting stars, star formation regions, and the generic distribution of other stellar populations in these galaxies is evident (Mahajan et al. 2022).

A significant finding with the *AstroSat*/UVIT is the discovery of a clumpy galaxy in *AstroSat* UV Deep Field (AUDF) named as AUDFs01 at redshift (z) of 1.42 close to the peak ($z \sim 1.6$) of the cosmic star formation history Saha et al. (2020). This is the first such galaxy to be found emitting Lyman continuum between $0.4 < z < 2.5$ (the "deserted" region for Lyman continuum leakers) and is a unique feature of UVIT. The amount of escaping Lyman continuum photons observed is a very important parameter in cosmological simulations and has a strong impact on processes leading to formation of galaxies.

There are several examples of joint observations with other observatories, and results published in the literature, which the readers can easily look up.

AstroSat is managed by the India Space Science Data Centre near Bengaluru. They schedule the operations of the satellite,

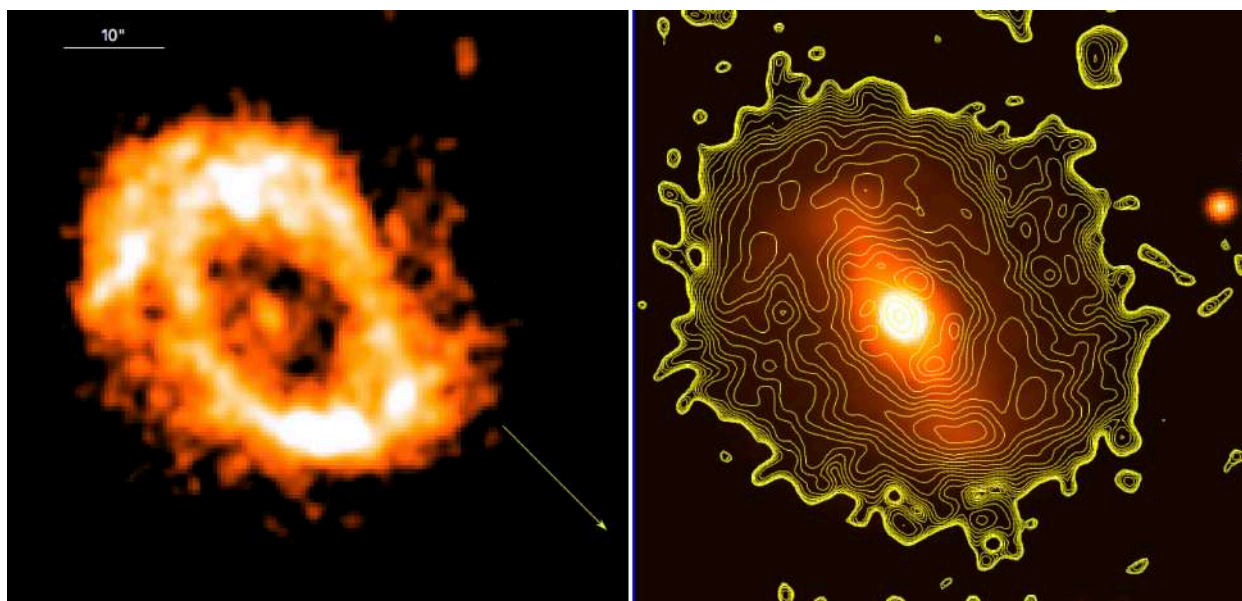


Figure 7: NGC4907 in Coma Cluster. (left) UVIT FUV image, and (right): the red-band optical image with an overlay of FUV contours. Credits: Mahajan et al. 2022

storage and dissemination of data in publicly available archives. Currently, *AstroSat* has fully active CPM, SXT and CZTI. The UVIT has only the FUV channel operating, LAXPC has one detector, and SSM has two detectors operating. So most of its multi-wavelength observing capability is still intact after 8 years of operations and *AstroSat* is expected to operate for as long as the conditions permit.

Bibliography

1. *AstroSat: I. The Scientific Instruments - AstroSat Payload*, Kulinder Pal Singh. Resonance, Vol. 27, pp. 513528 (2022). DOI: <https://doi.org/10.1007/s12045-022-1346-x>
2. *AstroSat: II. Highlights of Scientific Results From 2015 to 2021*, Kulinder Pal Singh. Resonance, Vol. 27, pp. 961981 (2022). DOI: <https://doi.org/10.1007/s12045-022-1391-5>
3. Vadawale S. V., Chattopadhyay, T., Mithun, N. P. S., et al, 2018, Nature Astronomy, Vol. 2, p. 50-55.
4. Husain, N. et al., 2023, MNRAS, 525, 4515.
5. Roy, P., Beri, A., & Bhattacharyya, S. 2021, MNRAS, 508, 2123.
6. Singh, K.P., et al, 2021, MNRAS, 501, 36.
7. Kumar, R., Pradhan, A.C., Mohapatra, A., et al., 2021, MNRAS, 502, 313.
8. Leahy D., Monaghan, C. and Ranasinghe, S. 2023, The Astronomical Journal, 165:116 <https://doi.org/10.3847/1538-3881/acb68d>

9. Mahajan, S. et al., 2022, Publications of the Astronomical Society of Australia, 39, e048. doi:10.1017/pasa.2022.45

10. Saha, K., Tandon, S. N. et al. 2020, Nature Astronomy, Vol. 4, p. 1185

Kulinder Pal Singh is currently INSA Senior Scientist at the Department of Physical Sciences at IISER Mohali. He joined TIFR as a graduate student in 1973 and continued to work there till 2017. He retired as a Senior Professor, Department of Astrophysics and Astronomy.

BETWEEN THE SCIENCE

ABHISHEK DHAR, received the prestigious J. C. Bose National Fellowship of the Science and Engineering Research Board (SERB), Department of Science & Technology, Government of India. He was also awarded the pan-TIFR TAA BM Udgaonkar: Excellence in Teaching Award for 2022 in Physics.

RAJESH GOPAKUMAR'S publication titled, *The Worksheet Dual of the Symmetric Product CFT*, in collaboration with Lorenz Eberhardt and Mattias R. Gaberdiel, received the 2023 ICBS Frontiers of Science Award, announced during the inaugural International Congress of Basic Sciences in Beijing in July 2023.

ICTS graduate student **SAHIL KUMAR SINGH** received the best poster award for his work titled, *Thermalization and Hydrodynamics in an Interacting Integrable System: The Case of Hard Rods*, presented at the recent School/Workshop on Wave dynamics: Turbulent vs Integrable Effects at ICTP, Trieste. The work was done in collaboration with Abhishek Dhar, Herbert Spohn, and Anupam Kundu.

PARAMESWARAN AJITH | *continued from Page 1 ...*

GRAVITATIONAL LENSING OF GRAVITATIONAL WAVES: A NEW FRONTIER OF ASTRONOMY

PARAMESWARAN AJITH



lensed quasar. These images are produced when a massive object (such as a galaxy or a cluster of galaxies) happens to lie in the line of sight of a distant source (such as a quasar or another galaxy).

Such a near-perfect alignment producing multiple images, called *strong lensing*, is rare. However, there are other forms of lensing. *Weak lensing*, in which the images of distant galaxies are distorted due to the presence of foreground galaxies or clusters is ubiquitous. Another regime of lensing is *microlensing*, where multiple images produced by a small and compact lens (such as a star or black hole) are too close to be resolved by any telescope. However, any relative motion between the source and the lens causes a time-dependent change in the observed flux, which can be used to identify microlensing.

Gravitational lensing has emerged as a powerful tool to probe the cosmos. GR provides an excellent theory of gravitational lensing. So, observations of lensed sources can be used to reconstruct the properties of the lensing object, even when it is invisible. Astrophysicists have used lensing observations to find evidence of dark matter and to probe its detailed nature, to detect planets outside the solar system, to observe the first galaxies and stars in the universe, to measure cosmic expansion rate, etc.

Gravitational-wave Astronomy

So far, GR has passed all the observational and experimental tests with flying colours. The most recent among them is the direct observation of gravitational waves (GWs) by the US-based LIGO observatories in 2016. Since then, LIGO and its sister European observatory Virgo have observed

about 100 GW signals from coalescing binaries of black holes and neutron stars from the distant universe.

Observations of GWs not only provide yet another confirmation of GR but also open up a new observational window to the cosmos. GW observations have provided evidence of merging binary black hole systems, mixed binaries involving neutron stars and black holes, a new population of massive stellar-mass black holes, hinted at the existence of intermediate-mass black holes, and provided constraints on the

equation of state of dense nuclear matter. The multi-messenger observation of the binary neutron star merger GW170817 enabled us to constrain several alternative theories of gravity, provided a new way of measuring cosmic expansion and provided tantalising hints of the origin of heavy elements in the universe.

GW astronomy is still in its nascent stages. LIGO and Virgo detectors are still reaching their design sensitivities. In the next few years, the KAGRA detector from Japan will join the network of ground-based GW

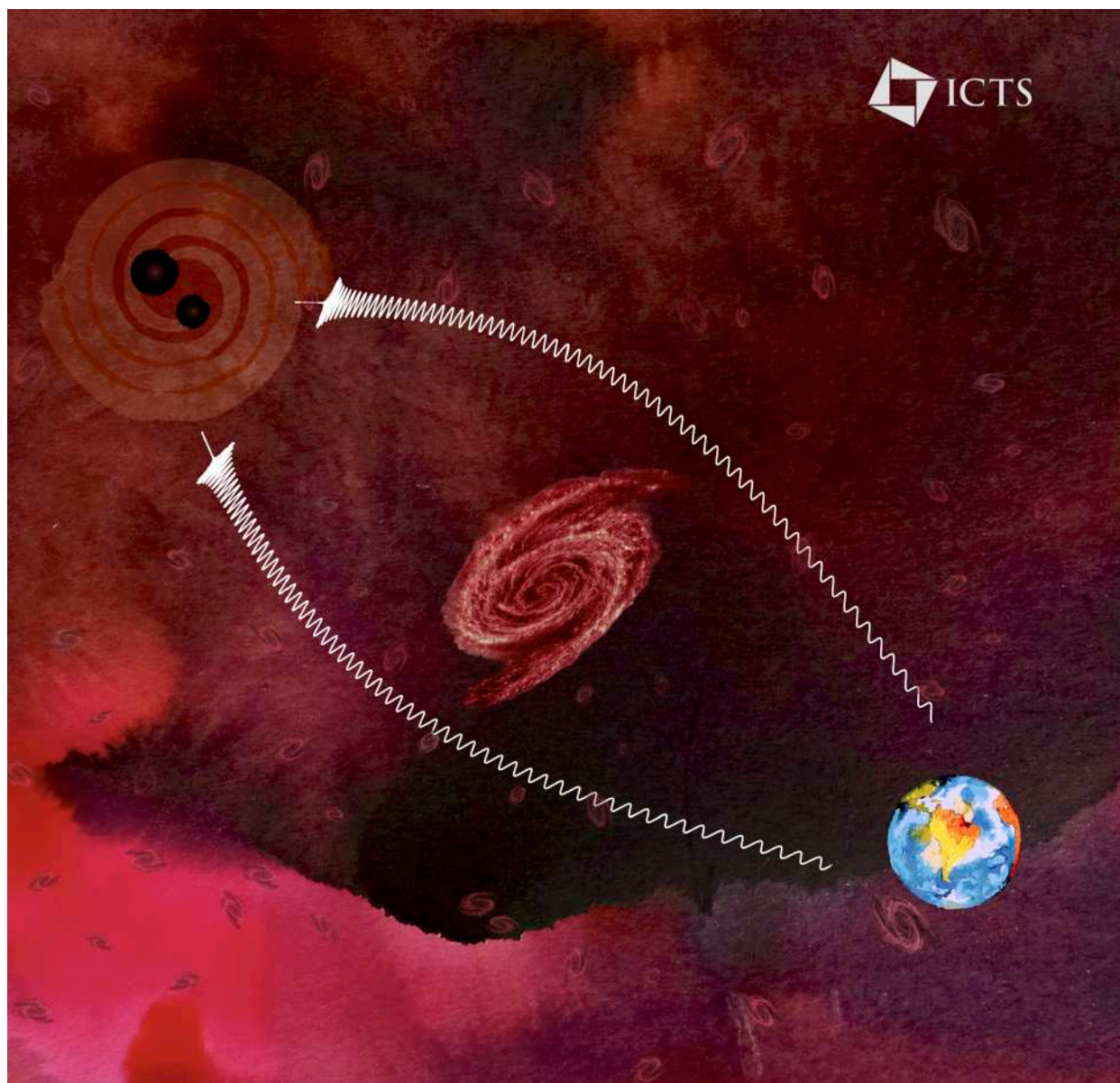


Figure 1: An artist's conception of the gravitational lensing of gravitational waves. The spacetime curvature caused by the galaxy in the middle causes the path of the gravitational waves to bend. Multiple paths from a given source can reach the observer, creating multiple copies of the signals. *Image: P. Ajith / ICTS.*

detectors. There is an ongoing effort to build a LIGO detector in India. Making use of the estimated merger rates of compact binaries in the universe, and the anticipated sensitivities of these detectors, it is safe to say that GW astronomers will observe thousands of binary mergers in the next decade. We are also likely to observe new phenomena, such as rapidly spinning neutron stars and core-collapse supernovae from our galaxy and an extragalactic GW background of many merging compact binaries.

Lensing of Gravitational Waves

Among the new phenomena that we expect to observe is the gravitational lensing of GWs. GR predicts that GWs will be lensed by intervening massive objects just like light. Galaxies and clusters remain the most likely lenses. Even though the GWs detected by ground-based detectors are of very long wavelength ($\sim 10^2\text{--}10^3$ km), it is still much smaller than the characteristic gravitational length scale of the galaxies and clusters ($GM_{\text{lens}}/c^2 \sim 10^{10}\text{--}10^{15}$ km). Hence lensing effects can be computed using the *geometric (ray) optics* approximation, where lensing can be modelled using the propagation of rays in a curved background, as done typically for the lensing of light.

Strong lensing by galaxies or clusters can produce multiple copies of the GW signals that are magnified differently, without distorting the shape of the signals. This is similar to the strong lensing of electromagnetic waves where different images are magnified differently, leaving their spectra unchanged. Each of these different copies picks up a distinct time delay while reaching the observer. This time delay is partly due to the longer distance the ray travels in a curved background (called *geometric delay*) and partly due to the gravitational time dilation due to the lensing potential (called *gravitational*, or *Shapiro delay*). This implies that the different lensed copies of the transient GW signals arrive at the detector at different times, separated by minutes to years.

Merging black hole binaries are *standard sirens* in GW astronomy (analogous to the *standard candles* in astronomy). The distance to the source can be accurately measured from the amplitude and shape of the observed signals. However, the magnification of the signals due to lensing

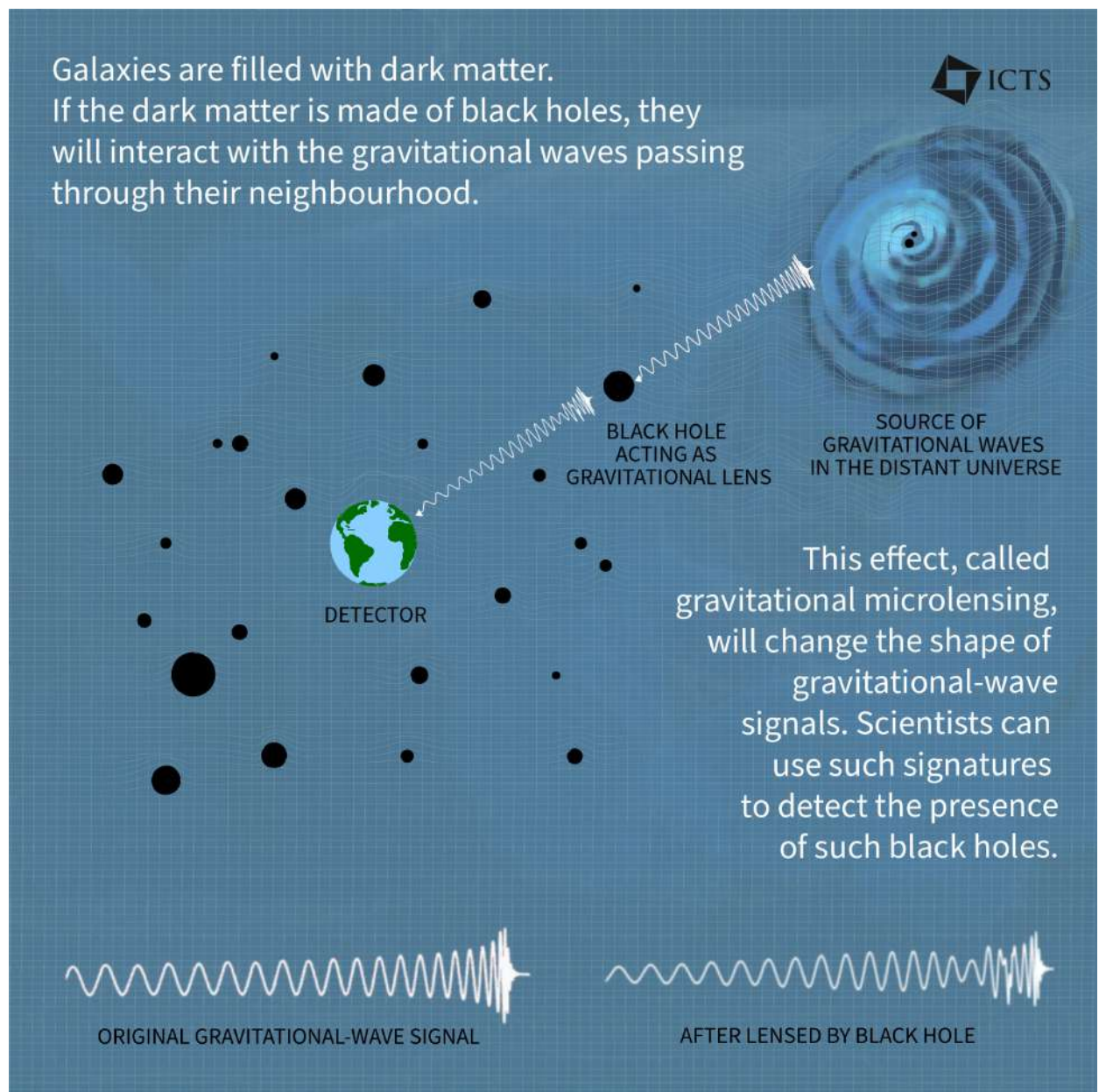


Figure 2: If a significant fraction of the dark matter is comprised of primordial black holes, GW signals from some of the distant sources will be gravitationally lensed by intervening black holes, introducing characteristic deformations in the observed signals. The non-observation of such deformations in a large number of GW signals can be used to constrain the abundance of primordial black holes. *Image: Roshni Samuel / P. Ajith / ICTS.*

will bias our distance estimation — lensed signals will be misidentified as unlensed signals coming from closer distances. Since the masses of merging black holes are estimated from the signal shape and the estimated distance, we will also incorrectly attribute higher masses to those black holes.

It is natural to wonder whether the high-mass black holes discovered through GW observations are in fact low-mass black holes — the kind of black holes from our own galaxy that we observe through X-ray telescopes — that are magnified by lensing. While a number of other observational and theoretical constraints make this very unlikely, one cannot rule out the possibility that at least some of the observed high masses are not artefacts of lensing

magnification.

The smoking gun evidence of GW strong lensing will be the observation of multiple copies of GW signals, analogous to the multiple images of quasars and galaxies that astronomers observe. We should look for multiple GW signals of similar shape coming from the same location in the sky, with time delays consistent with that expected from the known distribution of galaxies and clusters. Due to the rareness of lensed signals ($\sim 0.1\text{--}1\%$ of the total number of observed signals), the modest signal-to-noise ratios and the limited precision with which the signal properties can be estimated from the data, we will have to resort to statistical techniques for identifying lensed GWs. Bayesian model selection provides a powerful method.

Given a pair of observed signals, we can compute the *odds ratio* between the two alternative hypotheses: 1) that these pairs are lensed copies of the same signal, and 2) that these are two unrelated signals. Odds ratio is the ratio of the posterior probabilities of the two hypotheses, computed from the given data. Since the full calculation is computationally expensive, several approximations have been developed for this — some even using machine learning methods.

Searches in the data collected by LIGO-Virgo observatories during their first three observing runs haven't yielded any conclusive evidence of lensed GW signals. The non-observation of strongly lensed GWs can constrain the merger rate of binary black holes at high cosmological redshifts (equivalently, in the early universe). If the merger rate was high in the early universe, we should have already observed lensed GWs.

If the lensing object, such as a black hole, has a smaller characteristic size ($GM_{\text{lens}}/c^2 \sim 10^2\text{--}10^5\text{ km}$), then the *wave optics* effects such as diffraction, will be apparent. This will distort the GW signals, rendering the lensing effects identifiable. Due to the small wavelength of electromagnetic waves ($\sim 10^{-13}\text{--}1\text{ km}$), wave optics effects have not yet been observed in the gravitational lensing of electromagnetic waves. GW lensing will provide a unique opportunity to probe the wave optics regime of gravitational lensing.

The distortion of lensed GW signals due to wave optics effects can be modelled accurately for simple lens systems. One could employ Bayesian model selection techniques to identify such lensing signatures in the observed signals. The searches performed on the current LIGO-Virgo data have not yielded any strong evidence of wave optics effects in the observed GW signals.

This non-observation can be used to constrain the abundance of primordial black holes in the universe. These are black holes that *could be* produced in the early universe from the collapse of highly dense regions. Primordial black holes are possible candidates for dark matter. (Indeed, this possibility is heavily constrained by other astronomical observations, including the microlensing of electromagnetic waves.)

If the dark matter is mostly in the form of primordial black holes, GWs will be lensed by the black holes that they encounter as they (GWs) propagate to the earth (Figure 2). We have recently used the non-observation of such lensing signatures to constrain the fraction of dark matter in the form of black holes [*Basak et al ApJ Lett. 926, L28, 2022*]. Although the current constraints are modest, as the number of GW observations increases in the near future, these limits will become very interesting.

A New Tool for Astronomy

Since ground-based detectors are expected to observe thousands of GW signals in the next decade, we expect the first detection of lensed GWs to happen in the near future. These will provide a new tool for astronomers and cosmologists. Recent work has shown that lensed GWs will enable us to localise the binary black holes to their host galaxy — practically impossible to do otherwise due to the poor sky localisation of GW detectors. Identifying the host environments of binary black holes is a crucial step in understanding their (poorly understood) astrophysical formation mechanisms. On the other hand, if a strongly lensed binary merger has an electromagnetic counterpart, the host and lens galaxies can be identified. This will allow us to predict the arrival times of the next lensed images, providing early warning to electromagnetic telescopes.

Lensed GWs will provide new methods for cosmography. Multi-messenger observation of a lensed merger will enable us to measure the expansion of the universe, similar to what is attempted from lensed quasars. Recent work by our group at ICTS [*Jana et al, PRL 130, 261401 (2023)*] has shown that even in the absence of electromagnetic counterparts the fraction of lensed GW signals, the distribution of their lensing time delay and the deformation of the lensed signals will contain imprints of cosmological parameters and the nature of dark matter.

The first observations of the gravitational bending of light were performed as a means of testing the predictions of GR. Eventually, gravitational lensing emerged to be a powerful tool for astronomers and cosmologists. The first observations of lensed GWs are expected in the next decade, which will provide yet another

powerful tool to probe the cosmos.

Parameswaran Ajith is an astrophysicist and faculty member at ICTS-TIFR.

NON-NORMAL MATRICES: SPECTRAL INSTABILITY, PSEUDOSPECTRUM, AND RANDOM PERTURBATION

ANIRBAN BASAK



A finite dimensional matrix A is said to be normal or non-normal depending on whether $AA^* = A^*A$ or $AA^* \neq A^*A$, where A^* is the complex conjugate transpose of A . Spectral properties

of self-adjoint operators, the infinite dimensional version of finite dimensional matrices, or more generally that of normal operators are well understood due to the spectral theorem. Non-normal matrices and operators appear naturally in various branches of science, such as fluid dynamics, mathematical physics, partial differential equations, and many other fields, and

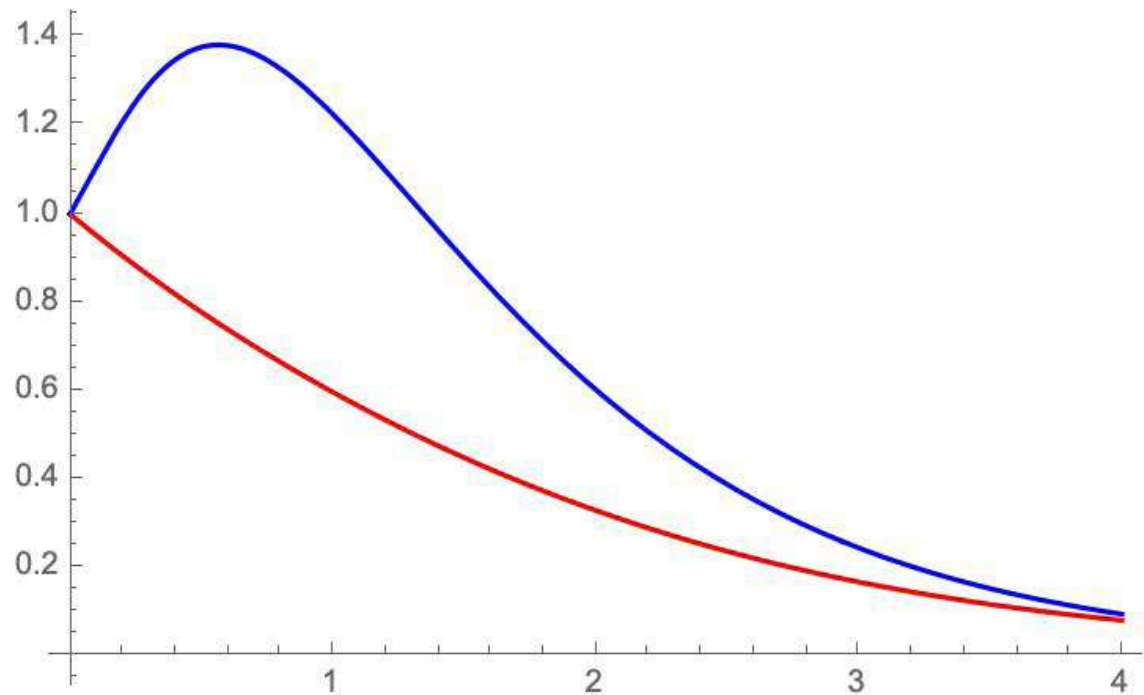


Figure 1

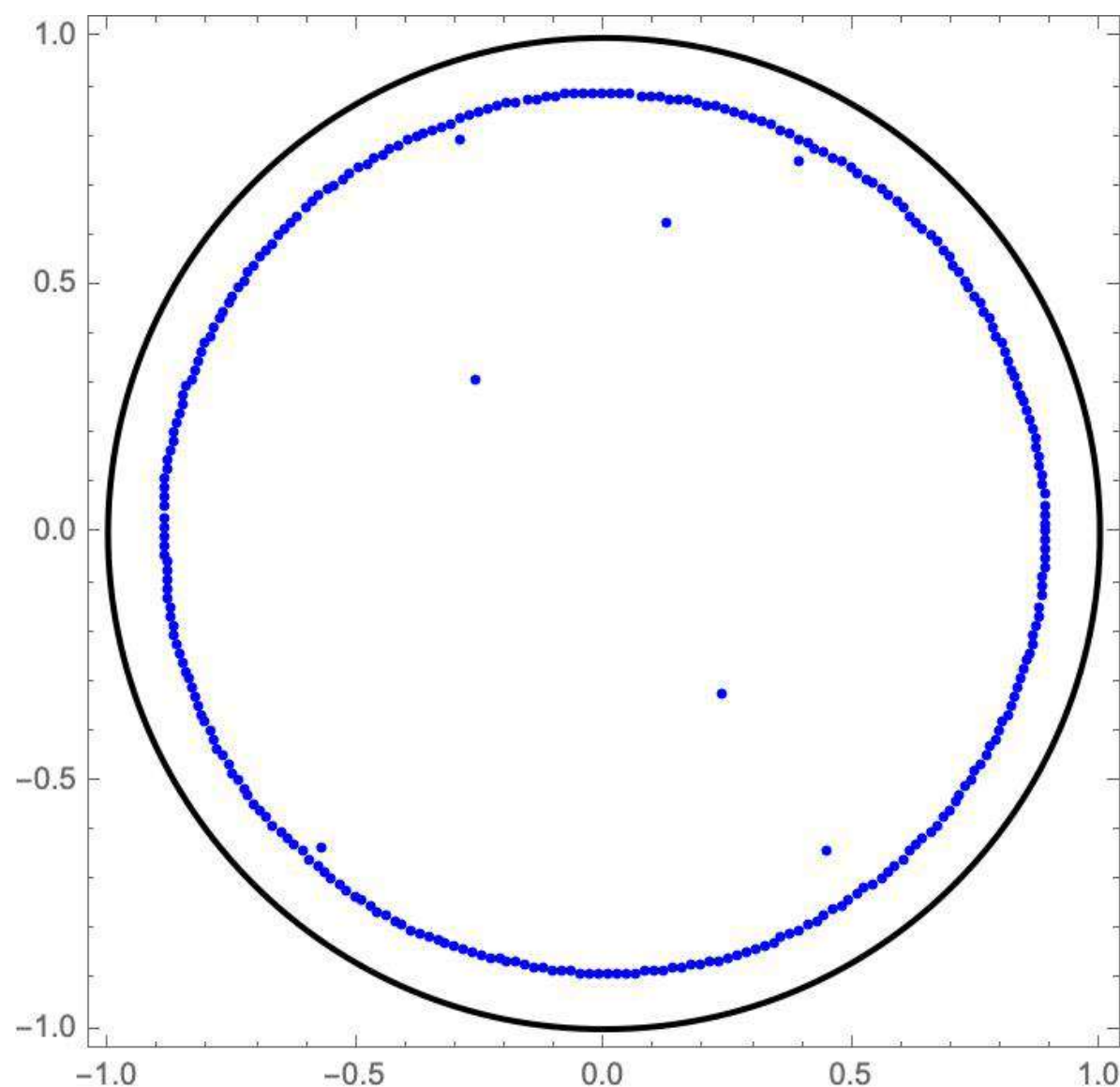


Figure 2

therefore their spectral properties need to be investigated. The absence of an analogue of the spectral theorem for non-normal operators makes the analysis of their spectral features challenging. On the numerical side, non-normal operators pose two major challenges: (i) the eigenvalue analysis in many applications turns out to be misleading, and (ii) the eigenvalues are sensitive to perturbations and thereby often yielding unreliable results. These two features are illustrated through the following two simple examples.

Example 1. Consider two matrices

$$A = \begin{pmatrix} -1 & 1 \\ 0 & -1 \end{pmatrix} \quad \text{and} \quad B = \begin{pmatrix} -1 & 5 \\ 0 & -2 \end{pmatrix}.$$

Set $f_A(t) = \|\exp(tA)\|$ and $f_B(t) = \|\exp(tB)\|$ for $t \geq 0$, where $\|\cdot\|$ denotes the operator norm. In Figure 1 the red and the blue curves represent f_A and f_B , respectively, as a function of t . For a large t , the slopes of these two curves can be determined via an eigenvalue analysis. However, the 'hump'-like structure in the blue curve cannot be explained solely by the eigenvalues of B . Such a hump-like structure is commonly known as the 'transient behavior' in the context of a dynamical system.

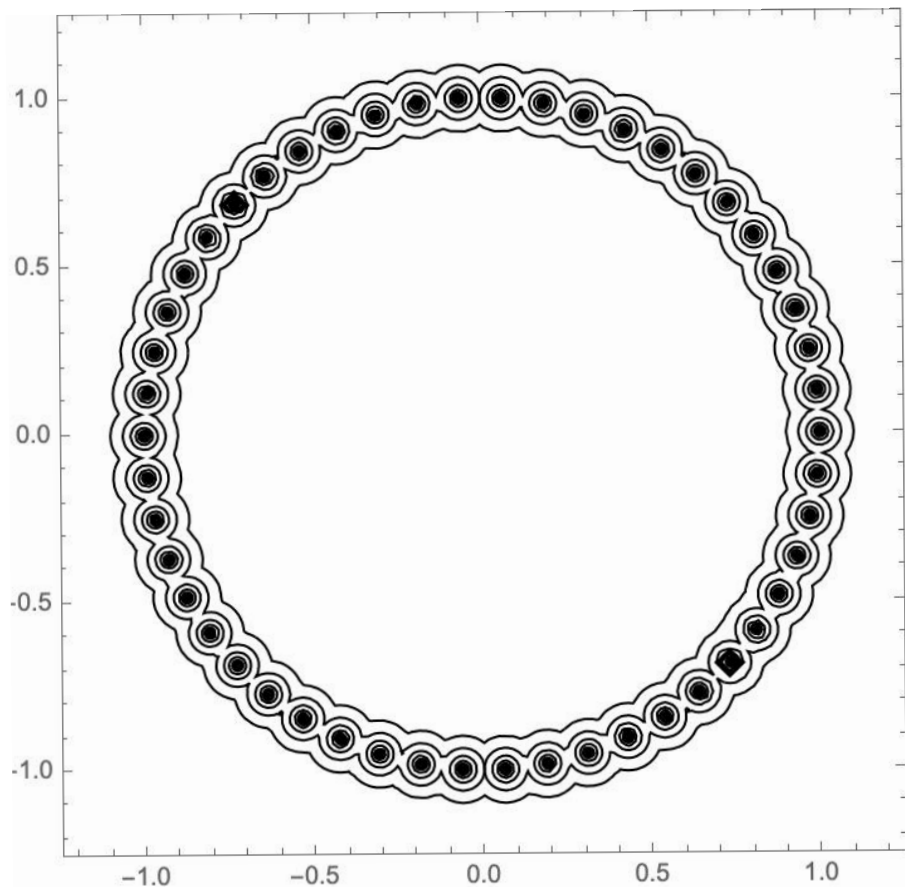


Figure 3

Example 2. Let J_N be the standard Jordan block of dimension N with zero on the diagonal. That is, the entries on the first super-diagonal position of J_N are one, and all other entries are zero. Simulate a uniformly random unitary matrix U_N and set $\hat{J}_N = U_N J_N U_N^*$. Clearly, the eigenvalues of J_N and \hat{J}_N are the same and are all equal to zero. However, when Mathematica is asked to compute the eigenvalues of \hat{J}_N it fails miserably to locate the correct eigenvalues. See Figure 2. Here $N = 1000$. The eigenvalues are plotted in blue and the unit circle \mathbb{S}^1 on the complex plane is drawn in black. Note that most of the eigenvalues computed through Mathematica are found near \mathbb{S}^1 . The most likely cause of this anomaly is the rounding or the machine error.

The notion of pseudospectrum offers an explanation to the phenomena seen in both Figures 1 and 2.

Pseudospectrum

For a finite dimensional matrix M its pseudospectrum is the collection of all $z \in \mathbb{C}$ such that the norm of $(z - M)^{-1}$ is large. More precisely, given an $\epsilon > 0$ the ϵ -pseudospectrum of M is set to be $\sigma_\epsilon(M) = \{z \in \mathbb{C} : \|(z - M)^{-1}\| \geq \epsilon^{-1}\}$.

Equivalently, $z \in \sigma_\epsilon(M)$ if and only if z

is in the spectrum of $M + E$ for some E such that $\|E\| \leq \epsilon$. The difference between the pseudospectrum of a normal and non-normal matrix is that for the former its ϵ -pseudospectrum is simply an $\epsilon > 0$ fattening of its spectrum. In contrast, the ϵ -pseudospectrum of a non-normal matrix, even for a tiny ϵ , may spread out over regions that are far from its spectrum. This is evident from Figures 3 and 4. These two plots show the ϵ -pseudospectral level lines for

$$\epsilon = 10^{-1}, 10^{-1.2}, \dots, 10^{-2},$$

and the eigenvalues for the matrices $C_N = J_N + E_N$ and J_N , respectively, where E_N is the N dimensional square matrix with one in its bottom left corner and zero elsewhere. The dimension $N = 50$.

The matrix C_N being a circulant matrix with its first row a canonical basis vector has its eigenvalues equispaced on \mathbb{S}^1 . It is a normal matrix. Note in Figure 3 that all its pseudospectral level lines are tightly knit around its eigenvalues. In contrast, ϵ -pseudospectral level lines of J_N are concentric circles with radii nearly equal to one, and thus are far away from the spectrum of J_N , which is Dirac at zero.

The book [TE05] is an excellent resource to learn about pseudospectrum, its properties,

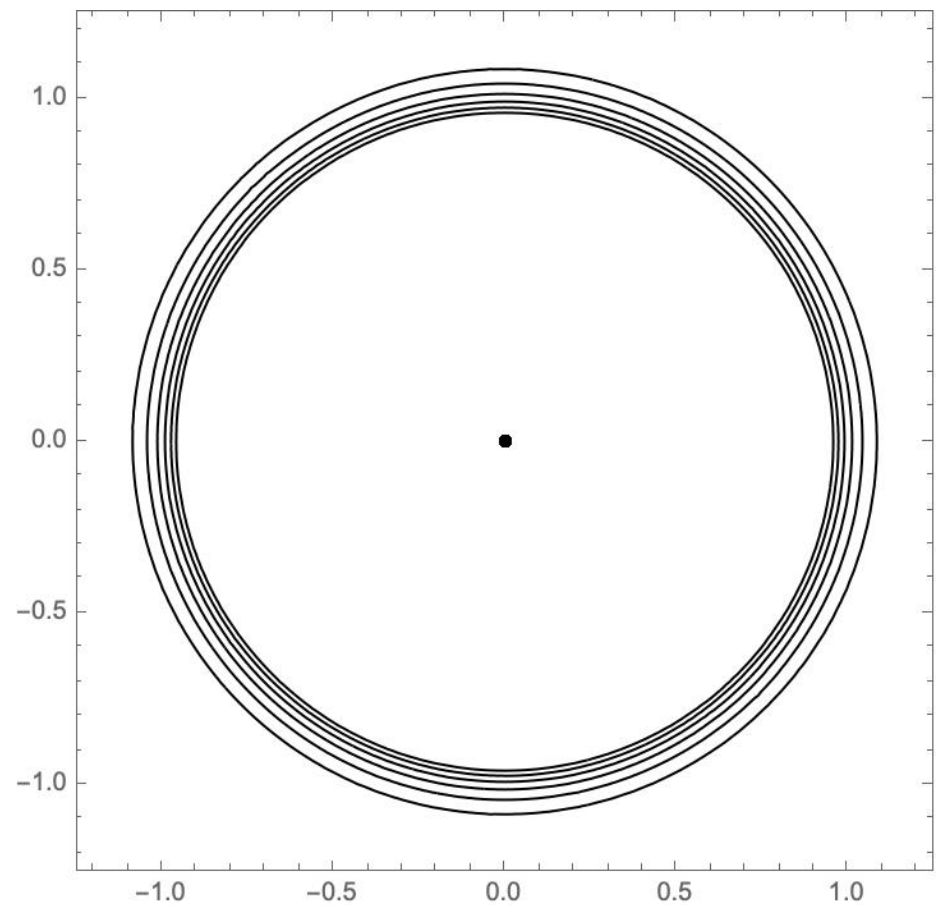


Figure 4

and its applications in and connections to various fields.

Let us return to Example 1. The eigenvalues of A and B are real and negative. Therefore, by standard linear algebra techniques $f_A(t), f_B(t) \rightarrow 0$ as $t \rightarrow \infty$. This is evident from Figure 1. To understand the hump-like structure of $f_B(t)$, as t varies, one needs to compare the pseudospectra of A and B . Figures 5 and 6 show the ϵ -pseudospectral level lines

$$\text{with } \epsilon = 10^{-0.2}, 10^{-0.4}, \dots, 10^{-1.2},$$

for A and B , respectively. The difference between these two sets of pseudospectral level lines is that the ones in Figure 5 do not protrude into the right half of the plane, while those in Figure 6 do. This last fact is indeed responsible for producing the hump-like structure of $f_B(t)$ for an intermediate range of t . See [TE05, Chapter 15] for further explanation and a proof.

A real life occurrence of the transient behavior shown through Example 1 is the onset of turbulence in the plane Couette flow at a high Reynolds number. The spectrum of the Navier-Stokes evolution operator linearized about the laminar flow is always contained in the left half of the plane. However, for a sufficiently large Reynolds number and a small $\epsilon > 0$ its ϵ -pseudospectrum protrudes a distance

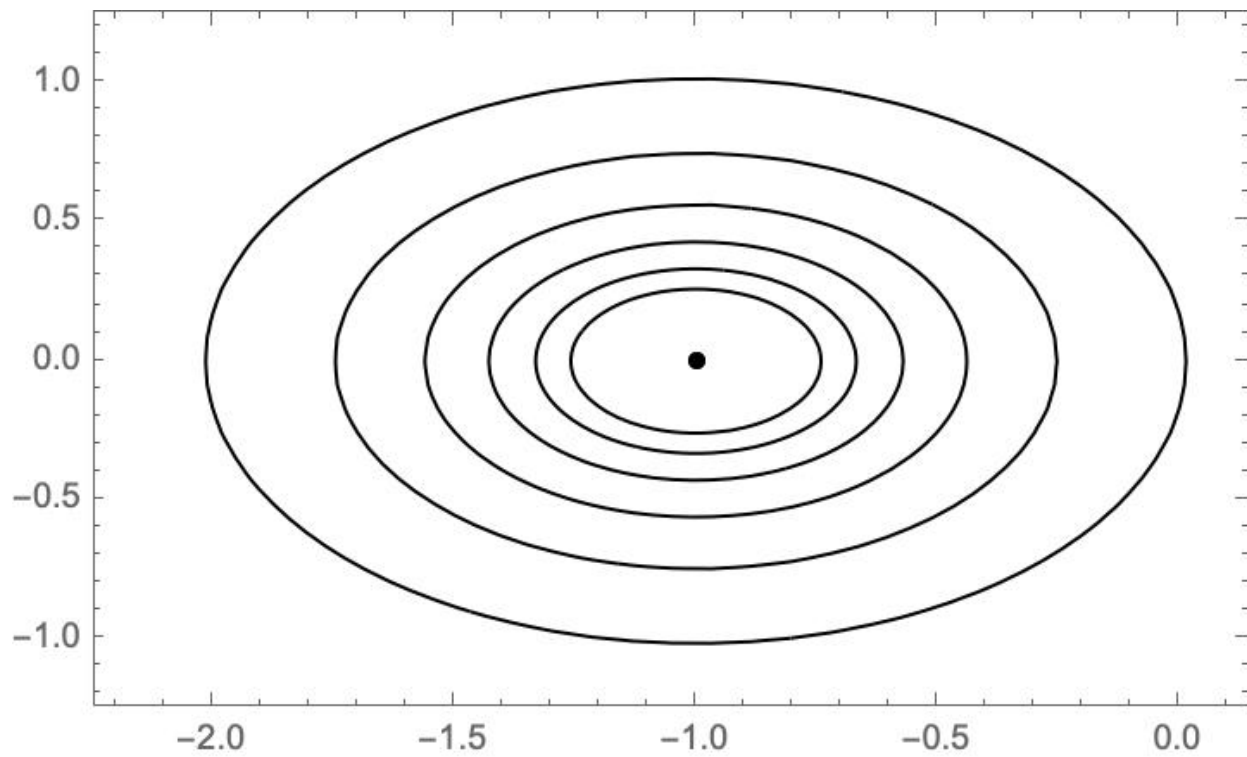


Figure 5

'much' greater than ϵ into the right half-plane, and as a result certain perturbations of the plane Couette flow grow transiently at that high Reynolds number eventually decaying due to viscosity.

We now return to Example 2. Due to machine errors we can think \hat{J}_N to be some additive perturbation of J_N . Since the machine errors are typically polynomial in the dimension, the eigenvalues of \hat{J}_N computed via Mathematica should be near the boundary of $\sigma_\epsilon(J_N)$, where ϵ is polynomially decaying in N . In Figure 4 we have seen that ϵ -pseudospectral level lines of J_N are merely concentric circles of varying radii depending on ϵ .

To understand how close these level lines can be to \mathbb{S}^1 consider $J_N + \epsilon E_N$, where E_N is as in the definition of C_N . Easy computations show that eigenvalues of $J_N + \epsilon E_N$ are equispaced on the circle of radius $\epsilon^{1/N}$. Thus, if ϵ decays polynomially in N , this radius would approach one as $N \rightarrow \infty$. This is precisely what we see in Figure 2 for almost all the eigenvalues \hat{J}_N computed through Mathematica.

Random Perturbation of Non-normal Matrices

The pseudospectrum of any matrix M measures how much one can move the spectrum of M under a 'worst'-case perturbation. However, in physical models the perturbation of an operator is generally induced by sources that are primarily uncontrolled by experimentalists.

Hence, instead of studying the spectral features of a worst-case perturbation of the operator in context, one is inclined to understand spectral features of disordered perturbations of a non-normal operators/matrices, e.g. open quantum systems. An early work in this direction was done by Hager [H06]. Since then there have been numerous works in understanding spectral features of random perturbations of non-self-adjoint (pseudo)-differential operators. In most cases researchers have studied the spectral density, and in some cases some finer features of the spectrum, such as the local spectral statistics, have been

obtained. The references [BMS10, CZ09, HS08, NV21] are some representative (non-exhaustive) works in this direction.

In the context of random perturbations of finite dimensional non-normal operators, i.e. non-normal matrices, most of the works have been for Toeplitz matrices, where a coherent theory have emerged over the last ten years.

Spectral Statistics of Random Perturbation of Toeplitz Matrices

Given a continuous function $\mathbf{a} : \mathbb{S}^1 \mapsto \mathbb{C}$ and $k \in \mathbb{Z}$ we write \mathbf{a}_k to denote the k -th Fourier coefficient of \mathbf{a} . An N -dimensional square matrix $T_N(\mathbf{a})$ is said to be a Toeplitz matrix of dimension N with symbol \mathbf{a} if $T_N(\mathbf{a})_{i,j} = \mathbf{a}_{i-j}$ for $1 \leq i, j \leq N$.

$T_N(\mathbf{a})$ is said to be finitely banded if $\mathbf{a}_k = 0$ for $|k| > K$, for some $K < \infty$ not depending on N . In that case, \mathbf{a} is a Laurent polynomial. The matrix J_N is a Toeplitz matrix with symbol $\mathbf{a}(\xi) = \xi$ with $\xi \in \mathbb{S}^1$.

Keeping in mind that in physical models the perturbations are typically polynomially vanishing in the dimension, we consider the random perturbation $T_N^\gamma(\mathbf{a}) = T_N(\mathbf{a}) + N^{-\gamma} G_N$, where G_N is random matrix and $\gamma > 0$ is known as the 'coupling constant'. A standard choice for G_N is the complex Ginibre matrix, i.e. all its entries are independent standard complex Gaussian random variables. Many of the results for $T_N^\gamma(\mathbf{a})$ allow the entries

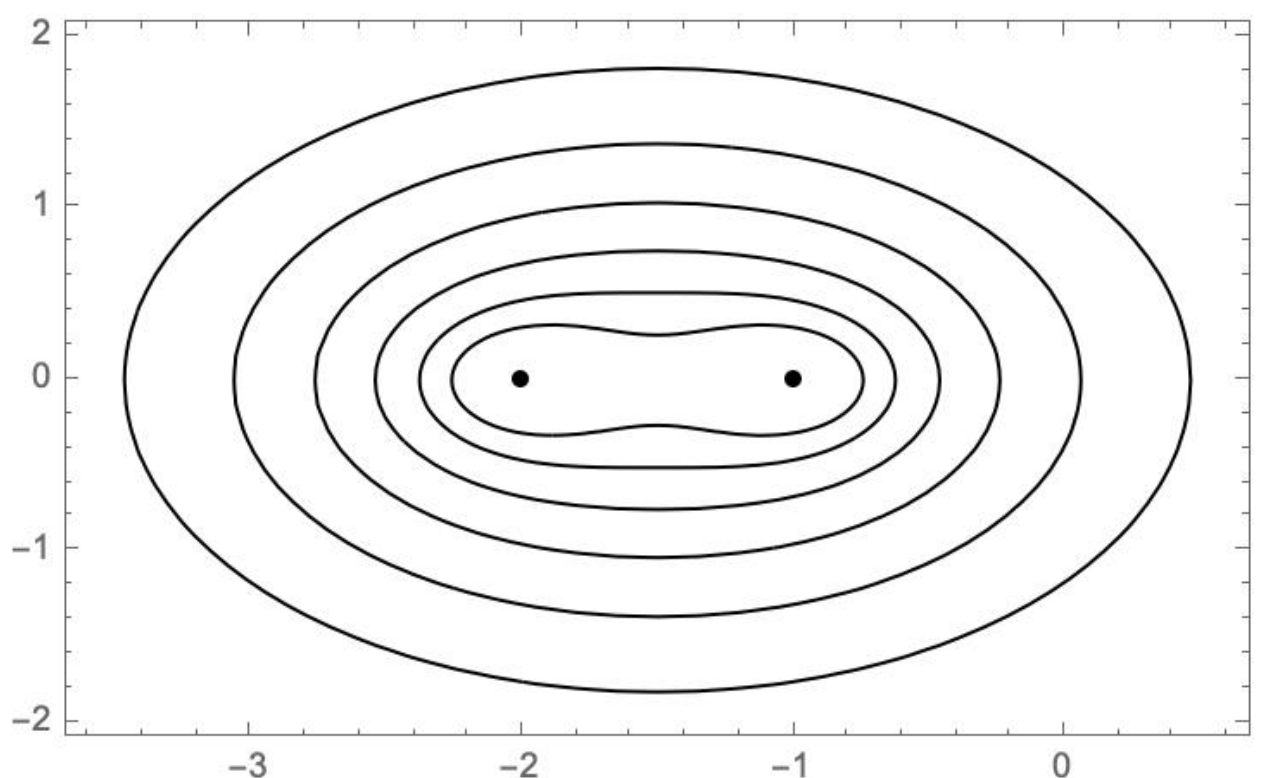


Figure 6

of G_N to have arbitrary distributions, e.g. discrete distribution supported on ± 1 , and some dependency among its entries. Let us also add that one needs to impose the lower bound $\gamma > 1/2$. Otherwise, the norm of $N^{-\gamma}G_N$ is too large so that $T_N^\gamma(\mathbf{a})$ can no longer be considered a perturbation of $T_N(\mathbf{a})$.

The first natural question to study is the asymptotic level density, or in the other words the limit of $L_N^\gamma(\mathbf{a})$, the empirical measure of the eigenvalues of $T_N^\gamma(\mathbf{a})$. It has been shown in [BPZ19, BPZ20, SV21] that as $N \rightarrow \infty$, the random probability measure $L_N^\gamma(\mathbf{a})$ converges weakly, in probability, to $\mathbf{a}_*(\frac{1}{2\pi}\text{Leb}_{\mathbb{S}^1})$, the push forward of the uniform measure on \mathbb{S}^1 by the symbol \mathbf{a} . In other words, the limiting distribution is induced by the distribution of $\mathbf{a}(U)$ where U is a random variable that is distributed uniformly on \mathbb{S}^1 . So in the case of J_N the limit is simply the uniform measure on \mathbb{S}^1 .

The above works also showed that the limit of $L_N^\gamma(\mathbf{a})$ is ‘universal’. That is, it does not depend on the coupling constant and on the distribution of the entries of G_N , as long as $\gamma > 1/2$. We remark in passing that

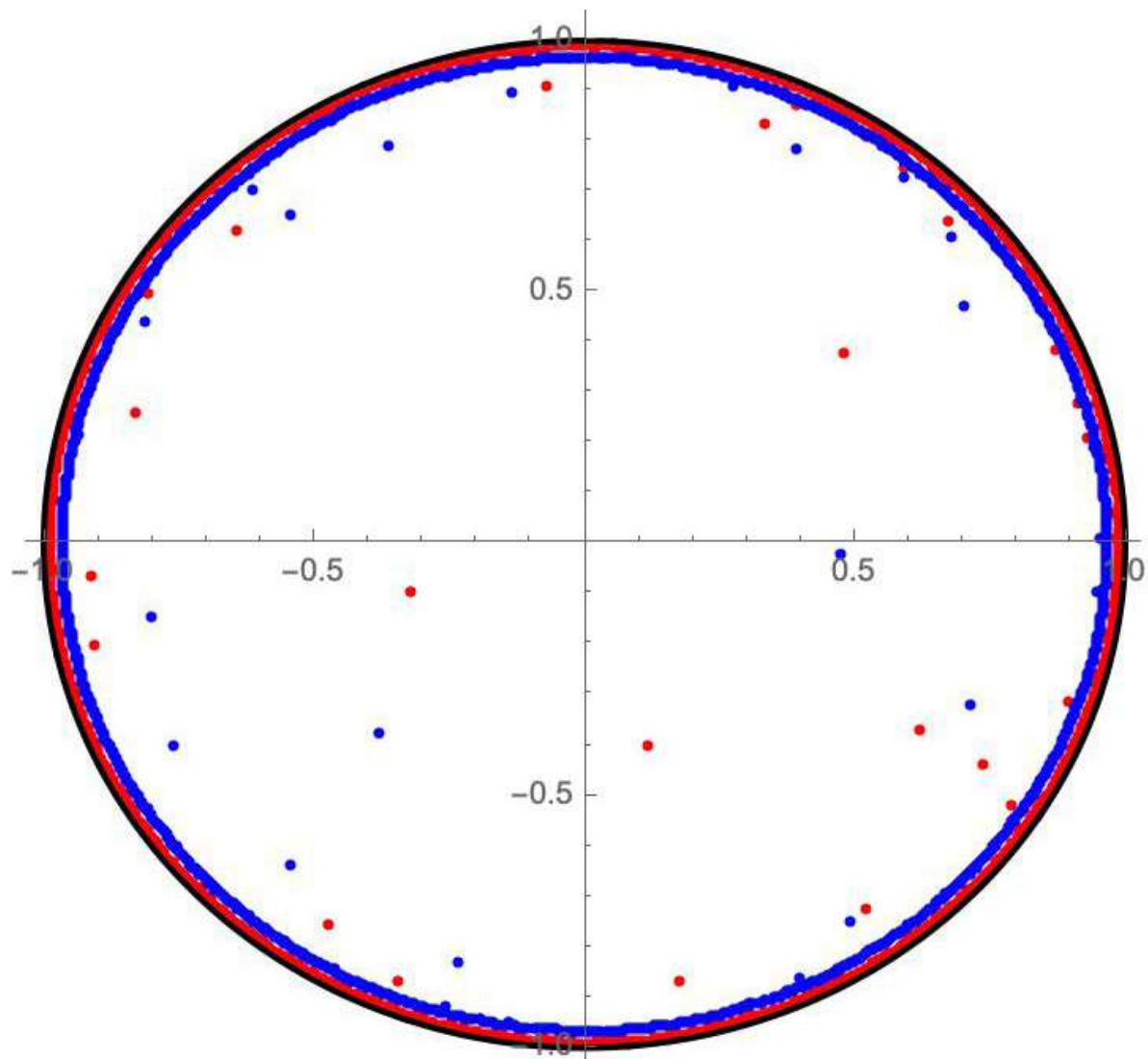


Figure 7

that the symbol curve, the support of the asymptotic level density, is the spectrum of the ‘limiting’ Laurent operator.

Having understood the limit of $L_N^\gamma(\mathbf{a})$, one is then inclined to understand finer details of the spectrum of $T_N^\gamma(\mathbf{a})$. The asymptotic level density tells us that most of the eigenvalues of $T_N^\gamma(\mathbf{a})$ approach the symbol curve $\mathbf{a}(\mathbb{S}^1)$ in the limit. Do *all* of them approach to $\mathbf{a}(\mathbb{S}^1)$? Are there regions in the complex plane where *no* eigenvalues are found with high probability? To understand these questions let us go through some simulations.

Figures 7 and 8 show the symbol curve (black) for two symbols, the eigenvalues of random perturbation of a Toeplitz matrix T_N associated with those symbols (red), and the eigenvalues of $U_N T_N U_N^*$ computed through Mathematica (blue), where U_N is a random unitary matrix. For Figure 7 the symbol $\mathbf{a}(\xi) = \xi$, i.e. the Toeplitz matrix is J_N , and in Figure 8 we have taken $\mathbf{a}(\xi) = 2\xi^{-3} - \xi^{-2} + 2i\xi^{-1} - 4\xi - 2i\xi^2$. $N = 1000$ and $\gamma = 2$ for both figures. It is instructive to note how close the three

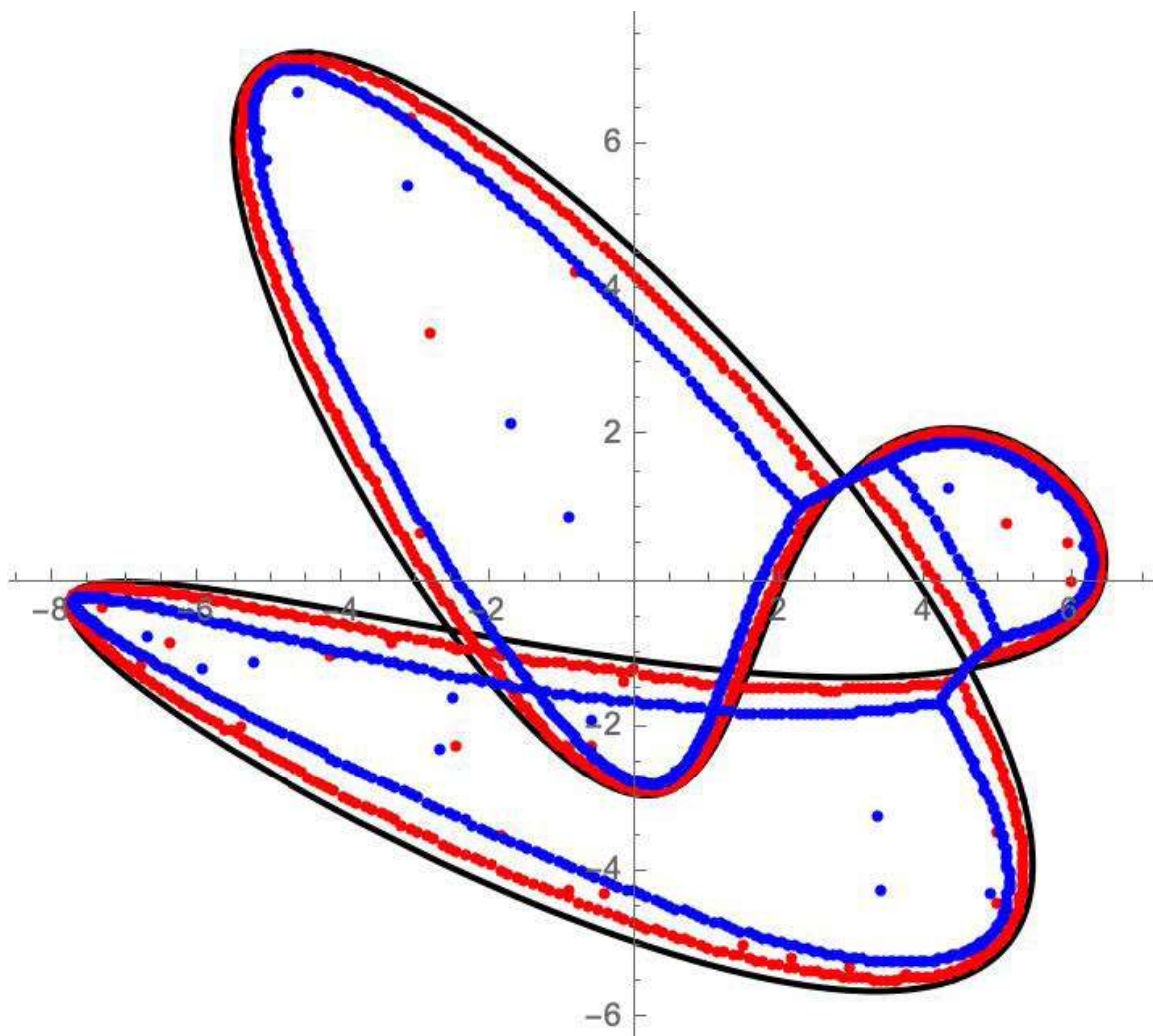


Figure 8

curves - the black, red, and the blue - are to each other, emphasizing yet again that random additive perturbation of non-normal matrices is a very good proxy for the machine errors.

Figure 7 shows that there are a handful of eigenvalues of the random perturbation of J_N that are 'strictly' inside unit disk and away from the symbol curve, while there are none outside the unit disk. Figure 8 throws at us another interesting behavior – there is a region enclosed by the symbol curve which do not seem to contain any eigenvalue at all.

These behaviors have been mathematically proven in [BZ20]. It was shown that any region of the complex plane that has a zero winding number with respect to the symbol curve $\mathbf{a}(\mathbb{S}^1)$ does *not* contain any eigenvalue with probability approaching one, as $N \rightarrow \infty$. Further the random point process obtained by those eigenvalues that are away from $\mathbf{a}(\mathbb{S}^1)$ has a limit given by the zero set of some random analytic function. For the simplest case of the Jordan block, when G_N is a complex Ginibre matrix, the limiting random analytic function turns to be a hyperbolic Gaussian analytic function. However, when the entries of G_N have a distribution other than Gaussian the limit is no longer a Gaussian random analytic function. This is different than the universality phenomenon noticed in the case of asymptotic level density.

For a general Toeplitz matrix, the limiting random analytic function possesses a rich structure. For example, for the Toeplitz matrix considered in Figure 8, even under a Gaussian perturbation, the limiting random function may not be even a Gaussian field. The Gaussianity property of the field in a region depends on its winding number w.r.t. $\mathbf{a}(\mathbb{S}^1)$. A full description of the field is beyond the scope of this article.

Recently localization properties of eigenvectors of $T_N^\gamma(\mathbf{a})$ have been studied in [BVZ23+], and for $\gamma > 1$ eigenvectors are shown to localize on sets of cardinality of the order $N/\log N$ and this is the scale where the eigenvectors spread out. The eigenvectors are predicted (through simulations) to undergo a phase transition $\gamma = 1$ and become delocalized for $\gamma < 1$.

The study of spectral properties of random perturbations of non-normal matrices/operators is still a relatively new and a

growing area. It is desirable to build a coherent theory that goes beyond the Toeplitz setting and allows us to understand the spectral properties of a random perturbation of a general non-normal matrix. For example, one would like to know whether the asymptotic level density can be read-off from the spectrum of the 'limiting' operator for any non-normal matrix with reasonable assumptions? Is the zone of zero winding number w.r.t. the symbol curve always free of stray eigenvalues? Are the eigenvectors always localized for a large γ ?

The approaches taken and the machineries used in the works mentioned above are very much Toeplitz specific. To address these questions in a general setting we need to bring in new ideas and machineries, and develop new methods.

References:

- [BPZ19] *Regularization of non-normal matrices by the Gaussian noise – the banded Toeplitz and twisted Toeplitz cases*, A. Basak, E. Paquette, and O. Zeitouni. Forum Math., Sigma, 7, paper e3, 2019.
- [BPZ20] *Spectrum of random perturbations of Toeplitz matrices with finite symbols*, A. Basak, E. Paquette, and O. Zeitouni. Trans. Amer. Math. Soc., 373(7), 4999–5023, 2020.
- [BVZ23+] *Localization of eigenvectors of non-Hermitian banded noisy Toeplitz matrices*, A. Basak, M. Vogel, and O. Zeitouni. Probab. Math. Phys., to appear.
- [BZ20] *Outliers of random perturbation of Toeplitz matrices with finite symbol*, A. Basak and O. Zeitouni. Probab. Th. Rel. Flds., 178(3), 771–826, 2020.
- [BMS10] *Weyl asymptotics for non-self-adjoint elliptic operators on compact manifolds*, W. Bordeaux Montrieux and J. Sjostrand. Ann Fac Sci. Toulouse, 19(3-4), 567–587, 2010.
- [CZ09] *Probabilistic Weyl laws for quantized tori*, T. J. Christiansen and M. Zworski. Commun. Math. Phys., 299, 305–334, 2009.
- [H06] *Instabilit e Spectrale Semiclassique d'Opérateurs Non-Autoadjoints II*, M. Hager. Ann. Henri Poincare, 7, 1035–1064, 2006.
- [HS08] *Eigenvalue asymptotics for randomly perturbed non-selfadjoint operators*, M. Hager and J. Sjostrand. Math. Ann., 342(1), 177–243, 2008.
- [NV21] *Local eigenvalue statistics of one-dimensional random nonselfadjoint pseudodifferential operators*, S. Nonnenmacher and M. Vogel. J. Eur. Math. Soc., 23(5), 1521–1612, 2021.

[SV21] *General Toeplitz matrices subject to Gaussian perturbations*, J. Sjostrand and M. Vogel. Ann. Henri Poincare, 22, 49–81, 2021.

[TE05] *Spectra and pseudospectra: the behavior of nonnormal matrices and operators*, L. N. Trefethen and M. Embree. Princeton University Press, 2005.

[V20] *Almost sure Weyl law for quantized tori*, M. Vogel. Commun. Math. Phys., 378(2), 1539–1585, 2020.

Anirban Basak is a mathematician and faculty member at ICTS-TIFR.

PROGRAMS

ICTP-ICTS Winter School on Quantitative Systems Biology

4-15 December 2023 ♦ Organizers — Vijaykumar Krishnamurthy (ICTS, India), Daniel Needleman (Harvard University, USA), Simone Pigolotti (OIST, Japan) and Shashi Thutupalli (ICTS/NCBS, India)
♦ Venue — Ramanujan Lecture Hall, ICTS

Algebraic and Combinatorial Methods in Representation Theory

13-24 November 2023 ♦ Organizers — B Ravinder (IIT Tirupati, India), R Venkatesh (IISc, India) and S Viswanath (IMSc, India)

Active Matter in Complex Environments

23 October-3 November 2023 ♦ Organizers — Poul H. Damgaard, Masanori Hanada, Anosh Joseph, Loganayagam R, Aninda Sinha and Toby Wiseman

IAGRG School on Gravitation and Cosmology

9-20 October 2023 ♦ Organizers — Amitabh Virmani (CMI, Chennai, India), Anjan Ananda Sen (CTP, Jamia Millia Islamia, New Delhi, India), Archana Pai (IIT Bombay, India), Sudipta Das (VBU, Santiniketan, India), Sudipta Sarkar (IIT Gandhinagar, India) and Parameswaran Ajith (ICTS-TIFR, Bengaluru, India)

Condensed Matter meets Quantum Information

25 September-6 October 2023 ♦ Organizers — Yuval Gefen (Weizmann Institute, Israel), Ganpathy Murthy (University of Kentucky, USA) and Sumathi Rao (ICTS-TIFR, India)

Bangalore School on Statistical Physics - XIV

11-22 September 2023 ♦ Organizers — Abhishek Dhar (ICTS-TIFR, India) and Sanjib Sabhapandit (RRI, India)

Rational Points on Modular Curves

11-22 September 2023 ♦ Organizers — Chandrakant Aribam (IISER Mohali, India), Shaunak Deo (IISc, India), Narasimha Kumar (Indian Institute of Technology Hyderabad, India) and Pierre Parent (Institute Mathematics De Bordeaux, France)

Statistical Methods and Machine Learning in High Energy Physics

28 August 2023 to 08 September 2023 ♦ Organizers — Sunanda Banerjee (University of Wisconsin, USA), Satyaki Bhattacharya (SINP, India), Indumathi D (IMSc, India), Bhawna Gumber (University of Hyderabad, India), Partha Konar (PRL, India), Aruna Kumar Nayak (IOPB, India) and Ritesh Kumar Singh (IISER, Kolkata, India)

Soft and Living Matter: from Fundamental Concepts to New Material Design

7-25 August 2023 ♦ Organizers — Mahesh M Bandi (Okinawa Institute of Science and Technology, Japan) and Ranjini Bandyopadhyay (RRI, India)

DISCUSSION MEETINGS

Field Theory and Turbulence

18-22 December 2023 ♦ Organizers — Katepalli R. Sreenivasan (New York University, USA), Loganayagam Ramalingam (ICTS-TIFR, Bengaluru, India), Luca Moriconi (UFRJ, Rio de Janeiro, Brazil) and Mahendra K. Verma (IIT Kanpur, India)

Lectures on Probability and Stochastic Processes XVI

17-21 November 2023 ♦ Organizers — Siva Athreya (ICTS-TIFR, ISI-Bengaluru, India), Nishant Chandgotia (TIFR-CAM, Bangalore, India) and Koushik Ramachandran (TIFR-CAM, Bangalore, India)

Active Matter and Beyond

6-10 November 2023 ♦ Organizers — Jean-François Joanny (Collège de France), Vijaykumar Krishnamurthy (ICTS, India), Cristina Marchetti (University of California, Santa Barbara, USA), Gautam Menon (Ashoka University, India and IMSc Chennai, India), Shraddha Mishra (Indian Institute of Technology (BHU), Varanasi, India), Madan Rao (NCBS, India) and Purna Sharma (IISc, India)

LIGO Science Workshop

27-28 October 2023 ♦ Organizers — Parameswaran Ajith (ICTS-TIFR, India), K. G. Arun (CMI, India), Bala Iyer (ICTS-TIFR, India), Shasvath Kapadia (IUCAA, India), Sanjit Mitra (IUCAA, India), Archana Pai (IIT Bombay, India) and Sendhil Raja (RRCAT, India)

LECTURE SERIES

INFOSYS-ICTS CHANDRASEKHAR LECTURES

The Allure of Active Matter

6-8 November 2023 ♦ Speaker — **Sriram Ramaswamy** (Honorary Professor and J C Bose National Fellow, IISc, India)

How materials can learn by themselves

21-23 August 2023 ♦ Speaker — **Andrea J Liu** (University of Pennsylvania, Philadelphia, USA)

PUBLIC LECTURES

On Quarks and Turbulence

20 December 2023 ♦ Speaker — **David Tong** (University of Cambridge)

DISTINGUISHED LECTURES

Exact Solution of Decaying Turbulence

19 December 2023 ♦ Speaker — **Alexander Migdal** (New York University, Abu Dhabi, UAE)

Duality in Condensed Matter Physics and Field Theory

27 September 2023 ♦ Speaker — **Eduardo H Fradkin** (University of Illinois at Urbana-Champaign, USA)

Statistical Mechanics of Mutilated Sheets and Shells

18 August 2023 ♦ Speaker — **David R. Nelson** (Lyman Laboratory of Physics, Harvard University)

EINSTEIN LECTURES

The Map of a Cat and Feynman's Other Intersections with Biology: Their Relevance for Today

26 November 2023 ♦ Speaker — **Shashi Thutupalli** (ICTS and NCBS, Bengaluru) ♦ **Kiru Rangamandira**, Mysore

KAAPI WITH KURIOSITY

Marine Living Resources: A Blue Future

10 December 2023 ♦ Speaker — **Sherine Sonia Cubelio** (Centre for Marine Living Resources & Ecology, Kochi) ♦ Venue — J. N. Planetarium, Bangalore

High Fidelity Sound Reproduction: Practical Aspects for the DIYer

19 November 2023 ♦ Speaker — **Reji Philip** (Raman Research Institute, Bengaluru) ♦ Venue — J. N. Planetarium, Bangalore

The Extreme Physics of Zombie Stars

8 October 2023 ♦ Speaker — **Nils Andersson** (University of Southampton) ♦ Venue — J. N. Planetarium, Bangalore

The Imaging Story: Black Holes to MRI

17 September 2023 ♦ Speaker — **Rajaram Nityananda** (ICTS-TIFR) ♦ Venue — J. N. Planetarium, Bangalore

The Odyssey of Liquid Crystals, From Carrot to Flat Screen

13 August 2023 ♦ Speaker — **Michel Mitov** (French National Centre for Scientific Research) ♦ Venue — J. N. Planetarium, Bangalore

Algebraic and Combinatorial Methods in Representation Theory

11-14 November 2023
Ramanujan Lecture Hall, ICTS Bengaluru

Minicourses (11 November to 14 November 2023)

Organizers: Indira Mukherjee (ICTS), Prakash Belkale (ICTS), Anurag Kulkarni (ICTS)

BIOENERGETICS

18-19 November 2023
Ramanujan Lecture Hall, ICTS Bengaluru

Organizers: Indira Mukherjee (ICTS), Prakash Belkale (ICTS)

Active Matter in Complex Environments

23 Oct - 3 Nov 2023
Ramanujan Lecture Hall, ICTS Bengaluru

Organizers: Indira Mukherjee (ICTS), Prakash Belkale (ICTS)

IAGRG SCHOOL ON GRAVITATION AND COSMOLOGY

02-20 OCTOBER 2023
RAMANUJAN LECTURE HALL, ICTS BENGALURU

LIST OF SPEAKERS: Prashant Shrivastava, Pradyumn Kumar, ...

Condensed Matter meets Quantum Information

28 Sept 2023 - 01 Oct 2023
Ramanujan Lecture Hall, ICTS Bengaluru

TOPICS: Foundations of quantum information, Quantum Hall effects, ...

Bangalore School on Statistical Physics - XIV

11 September - 22 September 2023
Vinnu, Ramana Research Institute, Bangalore

Organizers: Ashokh Dixit (ICTS) and Sushil Sakshapathi (IBR)

Rational Points on Modular Curves

11-22 September 2023
Ramanujan Lecture Hall, ICTS Bengaluru

List of Speakers: ...

STATISTICAL METHODS AND MACHINE LEARNING IN HIGH ENERGY PHYSICS

07-08 November 2023
Ramanujan Lecture Hall, ICTS Bengaluru

Organizers: Indira Mukherjee (ICTS), Prakash Belkale (ICTS)

Soft and Living Matter: from Fundamental Concepts to New Material Design

07-20 August 2023
Ramanujan Lecture Hall, ICTS Bengaluru

Organizers: Indira Mukherjee (ICTS), Prakash Belkale (ICTS)

Field Theory and Turbulence

18-22 December 2023
Ramanujan Lecture Hall, ICTS Bengaluru

Organizers: Indira Mukherjee (ICTS), Prakash Belkale (ICTS)

LECTURES ON PROBABILITY AND STOCHASTIC PROCESSES - XV

17-21 November 2023
Vinnu, Mathava Lecture Hall, ICTS Bengaluru

Organizers: Indira Mukherjee (ICTS), Prakash Belkale (ICTS)

Active Matter and Beyond

17-18 November 2023
Ramanujan Lecture Hall, ICTS Bengaluru

Organizers: Indira Mukherjee (ICTS), Prakash Belkale (ICTS)

LIGO Science Workshop

2023 Oct 27-28
ICTS Bengaluru

Organizers: Indira Mukherjee (ICTS), Prakash Belkale (ICTS)

THE ALLURE OF ACTIVE MATTER

08 November 2023, 10:00-11:30 AM
09 November 2023, 10:00-11:30 AM
10 November 2023, 10:00-11:30 AM
11 November 2023, 10:00-11:30 AM
12 November 2023, 10:00-11:30 AM
13 November 2023, 10:00-11:30 AM
14 November 2023, 10:00-11:30 AM
15 November 2023, 10:00-11:30 AM
16 November 2023, 10:00-11:30 AM
17 November 2023, 10:00-11:30 AM
18 November 2023, 10:00-11:30 AM
19 November 2023, 10:00-11:30 AM
20 November 2023, 10:00-11:30 AM
21 November 2023, 10:00-11:30 AM
22 November 2023, 10:00-11:30 AM
23 November 2023, 10:00-11:30 AM
24 November 2023, 10:00-11:30 AM
25 November 2023, 10:00-11:30 AM
26 November 2023, 10:00-11:30 AM
27 November 2023, 10:00-11:30 AM
28 November 2023, 10:00-11:30 AM
29 November 2023, 10:00-11:30 AM
30 November 2023, 10:00-11:30 AM
01 December 2023, 10:00-11:30 AM
02 December 2023, 10:00-11:30 AM
03 December 2023, 10:00-11:30 AM
04 December 2023, 10:00-11:30 AM
05 December 2023, 10:00-11:30 AM
06 December 2023, 10:00-11:30 AM
07 December 2023, 10:00-11:30 AM
08 December 2023, 10:00-11:30 AM
09 December 2023, 10:00-11:30 AM
10 December 2023, 10:00-11:30 AM
11 December 2023, 10:00-11:30 AM
12 December 2023, 10:00-11:30 AM
13 December 2023, 10:00-11:30 AM
14 December 2023, 10:00-11:30 AM
15 December 2023, 10:00-11:30 AM
16 December 2023, 10:00-11:30 AM
17 December 2023, 10:00-11:30 AM
18 December 2023, 10:00-11:30 AM
19 December 2023, 10:00-11:30 AM
20 December 2023, 10:00-11:30 AM
21 December 2023, 10:00-11:30 AM
22 December 2023, 10:00-11:30 AM
23 December 2023, 10:00-11:30 AM
24 December 2023, 10:00-11:30 AM
25 December 2023, 10:00-11:30 AM
26 December 2023, 10:00-11:30 AM
27 December 2023, 10:00-11:30 AM
28 December 2023, 10:00-11:30 AM
29 December 2023, 10:00-11:30 AM
30 December 2023, 10:00-11:30 AM
01 January 2024, 10:00-11:30 AM
02 January 2024, 10:00-11:30 AM
03 January 2024, 10:00-11:30 AM
04 January 2024, 10:00-11:30 AM
05 January 2024, 10:00-11:30 AM
06 January 2024, 10:00-11:30 AM
07 January 2024, 10:00-11:30 AM
08 January 2024, 10:00-11:30 AM
09 January 2024, 10:00-11:30 AM
10 January 2024, 10:00-11:30 AM
11 January 2024, 10:00-11:30 AM
12 January 2024, 10:00-11:30 AM
13 January 2024, 10:00-11:30 AM
14 January 2024, 10:00-11:30 AM
15 January 2024, 10:00-11:30 AM
16 January 2024, 10:00-11:30 AM
17 January 2024, 10:00-11:30 AM
18 January 2024, 10:00-11:30 AM
19 January 2024, 10:00-11:30 AM
20 January 2024, 10:00-11:30 AM
21 January 2024, 10:00-11:30 AM
22 January 2024, 10:00-11:30 AM
23 January 2024, 10:00-11:30 AM
24 January 2024, 10:00-11:30 AM
25 January 2024, 10:00-11:30 AM
26 January 2024, 10:00-11:30 AM
27 January 2024, 10:00-11:30 AM
28 January 2024, 10:00-11:30 AM
29 January 2024, 10:00-11:30 AM
30 January 2024, 10:00-11:30 AM
31 January 2024, 10:00-11:30 AM

HOW MATERIALS CAN LEARN BY THEMSELVES

Monday, 21 August 2023, 9:00 - 10:30
Tuesday, 22 August, 10:00 - 12:30
Wednesday, 23 August, 1:00 - 12:30

ANDREA J LIU
University of Pennsylvania, Philadelphia, USA

On Quarks and Turbulence

21-23 August 2023
RAMANUJAN HALL, ICTS, BENGALURU

4 pm, 20th Dec 2023
Chandrasekhar Auditorium, ICTS BIR, Bengaluru

David Tong
Imperial College London

Exact Solution Of Decaying Turbulence

19 December 2023, 4:00 pm-5:00 pm
RAMANUJAN HALL, ICTS, BENGALURU

Alexander Migdal
New York University, New York, USA

Duality in Condensed Matter Physics and Field Theory

27 September 2023, 4:00 pm-5:00 pm
RAMANUJAN HALL, ICTS, BENGALURU

Eduardo H Fradkin
University of Illinois at Chicago, Chicago, USA

Statistical Mechanics of Mutilated Sheets and Shells

18 August 2023, 3:30 pm-5:00 pm
RAMANUJAN HALL, ICTS, BENGALURU

David R. Nelson
Cornell University, Ithaca, New York, USA

Einstein lectures

Presented by: Shashi Thutupalli
University of Cambridge

The map of a cell and Feynman's other wanderings with Dookie, their adventures for today

Sunday, 26 November 2023
11:15 AM

KAAPI WITH KURIOSITY

Marine living resources: A blue future

Sherine Sonia Cubelio
4 PM, Sunday, December 10, 2023
Jawaharlar Nehru Planetarium, Bengaluru

LIVESTREAM ON YouTube

KAAPI WITH KURIOSITY

High Fidelity Sound Reproduction: Practical Aspects for the DIYer

Reji Philip
11 am, Sunday, November 19th, 2023
Jawaharlar Nehru Planetarium, Bengaluru

LIVESTREAM ON YouTube

KAAPI WITH KURIOSITY

The Extreme Physics of Zombie Stars

Nils Andersson
4 pm, Sunday, October 8th, 2023
Jawaharlar Nehru Planetarium, Bengaluru

LIVESTREAM ON YouTube

KAAPI WITH KURIOSITY

The Imaging Story: black holes to MRI

Rajaram Nityananda
4 pm, Sunday, September 17th, 2023
Jawaharlar Nehru Planetarium, Bengaluru

LIVESTREAM ON YouTube

KAAPI WITH KURIOSITY

The odyssey of liquid crystals from carrot to flat screen

Michel Mitov
4 pm, Sunday, Aug 13th, 2023
Jawaharlar Nehru Planetarium, Bengaluru

LIVESTREAM ON YouTube

ICTS NEWS

INTERNATIONAL
CENTRE *for*
THEORETICAL
SCIENCES

VOLUME IX
ISSUE 2
2023

TATA INSTITUTE OF FUNDAMENTAL RESEARCH

PAGE 1

ASTROSAT: EIGHT YEARS ON AND
COUNTING!

PAGE 1

GRAVITATIONAL LENSING OF
GRAVITATIONAL WAVES: A NEW
FRONTIER OF ASTRONOMY

PAGE 9

NON-NORMAL MATRICES:
SPECTRAL INSTABILITY,
PSEUDOSPECTRUM, AND RANDOM
PERTURBATION

